Chunxiang Chen, Qing Nian Chan, Paul R. Medwell and Guan Heng Yeoh

Co-combustion characteristics and kinetics of microalgae chlorella vulgaris and coal through TGA

Combustion Science and Technology, 2020; 192(1):26-45

Published online: 26 Dec 2018

Co-combustion characteristics and kinetics of microalgae *Chlorella vulgaris* and coal through TGA

Chunxiang Chen[a*], Qing Nian Chan[b], Paul R. Medwell[c] and Guan Heng Yeoh[b]

[a]College of Mechanical Engineering, Guangxi University, University Road 100, Xixiangtang District, Nanning City, 530004, PR China.

[b]School of Mechanical and Manufacturing Engineering, The University of New South Wales, Sydney, NSW 2052, Australia.

[c]School of Mechanical Engineering, The University of Adelaide, Adelaide, SA 5005, Australia.

Abstract

The combustion characteristics and kinetics of microalgae (*Chlorella vulgaris*) and sub-bituminous coal blends (CCBs) are studied by a thermogravimetric analyzer (TGA), and those of pure *Chlorella vulgaris* (*C. vulgaris*) and coal were also taken respectively as control groups. The microalgae to coal blending ratio (MCR) is 3/7, 5/5 and 7/3. The results showed that three stages were observed during the combustion of CCBs. And the main combustion of CCBs was occurred at the second stage ranged from 254.6~ 389.4°C to 698.7~ 741.0°C. Both of T_i and T_f were decreased as the *C. vulgaris* content increased in the CCB. R_{max} of *C. vulgaris* was maximum. R_v was firstly decreased, and then increased as the content of *C. vulgaris* in CCBs increasing. With the increasing content of *C. vulgaris*, both of D_i and S_M were increased. Some deviations from their expected characteristics indicate interaction. As β increases, T_i,

* Corresponding author. Tel: 0086 771 3232294; fax: 0086 771 3232294
E-mail: xiangxiang570@163.com (C.X. Chen).

T_p, R_p ,R_v and T_f were all increased significantly, while M_r was first increased, and then decreased. For CCBs, E was the first decreased, and then increased, and the minimum E was obtained as MCR= 5/5. Among all the samples, E of pure coal was the minimum one. Finally, kinetic triplets were determined by the Kissinger–Akahira–Sunose (KAS), Flynn–Wall–Ozawa (FWO), and master-plots method.

Key words: Microalgae; *Chlorella vulgaris*; Co-combustion; Coal; Thermogravimetric analysis (TGA)

1 Introduction

Driven by the depletion of world's energy reserves and ever-increasing fuel prices, in addition to the challenges of limiting global warming, there is a strong motivation to seek alternative renewable energy resources, such as biomass fuels. The utilization of biomass fuels for power generation is attractive as they offer potential benefits in reducing greenhouse gas emissions, and in substituting part of the conventional energy sources [1].

Microalgae [2] are widely considered as one of the most promising sources of biomass [3]. The use of microalgae as the biomass feedstock is attractive as they have huge carbon abatement volume, in addition to faster growth rates and higher yields, when compared with other potential biomass feedstock, such as terrestrial plants [4]. Many microalgae can also be cultivated in less arable land [5]. Moreover, unlike some other forms of biomass, microalgae production has limited impact on the utilization of land and resources otherwise used for food production. *Chlorella vulgaris* (*C. vulgaris*) is a species of *Chlorella* [6], and is widely considered as one of the most

promising sources of biomass, ever since its first large-scale culture at Japan in the early 1960s [7]. This microalgae species is therefore selected for the purpose of this study.

Combustion is one of the most important and mature pathways to extract energy from various fuel sources [8]. The direct combustion of microalgae biomass in existing power plants for power generation is an attractive option [9], as it can offer potential economic benefit through reduced infrastructure investment, in addition to the environmental benefits that it can bring. It is therefore important to understand the combustion characteristics of microalgae, which is the one main aims of this work.

The co-combustion of biomass with fossil fuel resources, such as coal, is another attractive option that can lead to environmental, technical and economic benefits [6,10]. The co-combustion of the blends can help to reduce the consumption of non-renewable fossil fuels for power generation [11]. Furthermore, existing fossil fuel powered plants may continue to be used with few modifications, when the co-combustion option is implemented [12]. The differences in the composition and the heating properties of the biomass and fossil fuels [13] also provide opportunities for synergy to be achieved [3] during the co-combustion of the blends. For example, Wang et al.[14] reported that the mixing of biofuel with coal can be used to achieve a more continuous heat release from the corresponding combustion process. Previous studies have also demonstrated that the fouling and ash deposition problems on convective heating surfaces, which are typically encountered during the combustion of biomass, can be alleviated through co-firing [15]. The co-combustion of

sub-bituminous coal with biomass in power stations has also been reported to display synergetic effect of reducing the greenhouse gases emissions per unit of energy produced [16] when compared with the combustion of pure coal. In view of all these aforementioned factors, a more detailed understanding of the thermal characteristics and kinetics of the microalgae/coal blends, is essential. on the other hand, the combustion kinetic information of the fuels, provides critical information that is needed for modelling studies, which are required for fine-tuning the operation of the corresponding systems.

At present, the study of microalgae is more focused on the microalgae cultivation [17-18], pyrolysis [5-6,19-21] and comparison between the pyrolysis and the combustion in air atmosphere [22] and comparison between the combustion in 20%O_2/80%N_2 with 20%O_2/80%CO_2 atmospheres [23] and comparison the combustion under different oxygen supply concentrations in an O_2/N_2 atmosphere [24]. Besides, the co-combustion characteristics of microalgae and coal under O_2/N_2 and O_2/CO_2 atmospheres were also studied by using the thermogravimetry. Reference [25] mainly studied the difference of combustion characteristics (ignition temperature, burnout temperature, peak temperature and maximum weight loss rate) and kinetic (activation energy E) of microalgae/coal blends in different atmospheres (O_2/N_2 and O_2/CO_2 atmosphere). Reference [26] mainly studied the effect of oxygen concentration on microalgae combustion and compared the characteristic parameters (ignition temperature, peak temperature, maximum weight loss rate and E) of microalgae/ coal blends under O_2/N_2 atmospheres with O_2/CO_2 atmosphere. However,

the comprehensive combustion characteristics and the combustion kinetic triplets of microalgae/ coal blends at different blending ratios have not been reported yet.

This work is to characterize the combustion behavior of microalgae (*C. vulgaris*), sub-bituminous coal and their blends by a thermogravimetric analyzer (TGA) in an 21%O_2/79%N_2 atmosphere. The effects of *C. vulgaris*/coal blending ratios (3/7, 5/5 and 7/3) and heating rates (βs) (10, 20, and 40°C/min) on the combustion of the samples are studied. The ignition index (D_i) and the comprehensive combustion characteristic index (S and S_M) are used to evaluate the combustion characteristics of the fuels. The interaction of *C. vulgaris* and coal during co-combustion is investigated. In addition, the combustion kinetic triplets (E, n and A) of pure *C.vulgaris*, coal and their blends are studied by the Kissinger–Akahira–Sunose (KAS), Flynn–Wall–Ozawa (FWO) and master-plots method. The critical information generated will guide the operation or future design of combustion units utilizing the co-combustion of microalgae and coal.

2 Materials and methods

2.1 Materials

The powder of *C. vulgaris* and sub-bituminous coal (low rank) are respectively provided by Jiangmen Yue Jian Biotechnologies Co, Ltd. (Guangdong Province, China) and Lingli Sugar Refinery and Power Plant located at Nanning (Guanxi Zhuang autonomous region, China). These two samples are used in this study. The coal is difficult to fire and burn and its C/H are about 13.96 which are much higher than *C.*

vulgaris (7.46). Thus, it was chosen to blend with *C. vulgaris*. The samples of *C. vulgaris* and coal were prepared by pulverization in a mortar to be small enough to eliminate the heat transfer effects and dried at 105 °C for 24 hours, and then blended complying with the ratios of 3/7, 5/5 and 7/3 in weight by tumbling for 2 hours to achieve proximate homogeneity. Finally, the powder of CCB, pure *C. vulgaris* and pure coal were sieved to achieve a size-range less than 200μm.

The ultimate analysis, proximate analysis and lower heating values of samples were carried out through Vario EL-II chons elemental analyzer (Elementar Analysen systeme Gmbh, Germany), MA260S electronic balance (Shanghai Second Balance Instrument Factory, Shanghai, China) and Parr 6300 oxygen bomb calorimeter (PARR instrument company, America) correspondingly. The results are shown in Table 1. From Table 1 it can be seen that the proximate and ultimate analyses results and lower heating values of *C. vulgaris* and coal differ considerably.

2.2. Experimental Methods

Combustion tests were performed using a thermogravimetry analyzer (American TA Q500) that can measure a maximum sample weight of 1g, with a sensitivity of 0.1 μg. Schematic diagram of the experimental setup used for thermogravimetric analysis is shown in Fig.1. The tests were performed at atmospheric pressure condition and under artificial air environment. Carrier gas with a gas composition of 21% oxygen and 79% nitrogen (by volume), was introduced into the analyzer at a fixed flow rate of 100mL/min throughout the experiments, to simulate air condition.

All samples were initially heated from 40 to 105°C, under which they were held for 10 minutes to ensure that all parts of the samples were of the same initial temperature value, prior to the start of the experiments. Each sample was then heated up to 900°C at three different βs of 10, 20 and 40 °C/min, respectively. To minimize the effects of heat and mass transfer limitations [24], small sample masses (10±0.1 mg) were used for the experiments.

3 Data Analysis Methodologies

3.1 Characterization of Ignition and Combustion Properties

In order to evaluate the ignition and the combustion characteristics of the fuels, the ignition index D_i (%/min), and the comprehensive combustion characteristic index S (%^{2}/(min^2/°C^3)) of the samples were computed using expressions. The D_i [27] was calculated using:

$$D_i = R_{max} t_i / t_m \tag{1}$$

where R_{max} (%/min) is the maximum combustion rate, t_i (min) is the ignition time that corresponds to ignition temperature T_i (°C), and t_m (min) is the time, which corresponds to R_{max}. The T_i values of the fuels were derived from their combined weight loss (TG) and rate of weight loss (DTG) plots, following the approach of Pu et al [28].

The S [28] was calculated using:

$$S = R_{max} R_v / (T_i^2 T_f) \tag{2}$$

where R_v (%/min) is the average mass loss rates and T_f (°C) is the burnout temperatures. The burnout temperature of the sample is defined here as the

temperature value at which the weight of the fuel is found to stabilize in its TG plot.

The combustion characteristic index S, however, is not applicable for biomass/coal blends, especially combustion index of blends S was used in this study in order to evaluate the combustion behavior of the blends and eliminate the effects caused by different blend ratios, and revised as follows [28]:

$$S_{\mathrm{M}} = \frac{\sum_{j=1,2} R_{\mathrm{pj}}}{2} R_{\mathrm{v}} / (T_{\mathrm{i}}^{2} T_{\mathrm{f}}) \tag{3}$$

The first item in the numerator is the arithmetical average value of the maximum mass loss rates in the volatile release region (R_{p1}) and in the fixed carbon combustion region (R_{p2}), respectively.

Higher values of D_{i}, S or S_{M} are typically indicative of fuel with better ignition and combustion performances.

3.2 Kinetic Analysis

The rate of homogeneous solid-state reactions is generally represented using:

$$d\alpha / dt = A \exp(-E / RT) f(\alpha) \tag{4}$$

where α is the conversion degree of the material, t (min) is time, A (min^{-1}) is the Arrhenius pre-exponential or frequency factor, E (kJ/mol) is the activation energy, R (kJ/mol·K) is the universal gas constant and T (K) is the absolute temperature. In addition, $f(\alpha)$ is the reaction model function that is dependent on the reaction mechanism involved, and is represented as:

$$f(\alpha) = (1-\alpha)^{n} \tag{5}$$

where n is the reaction order.

Noting that the heating rate β (°C/min) of the sample is defined as:

$$\beta = dT / dt \tag{6}$$

Eq. (4) can therefore be rewritten as:

$$d\alpha / (1-\alpha)^n = A / \beta \exp(-E / RT) dT \tag{7}$$

or when expressed in an integrated form ($g(\alpha)$):

$$g(\alpha) = \int_0^{\alpha} d\alpha / (1-\alpha)^n = A / \beta \int_{T_0}^{T} \exp(-E / RT) dT \tag{8}$$

The temperature expressions can be represented using:

$$T = T_0 + \beta t \tag{9}$$

where T_0 refers to the initial temperature [29]. The degree of conversion of the material (α) is defined as [30-31]:

$$\alpha = (m_{\mathrm{i}} - m_{\mathrm{t}}) / (m_{\mathrm{i}} - m_{\infty}) \tag{10}$$

where m_{i}, m_{t} and m_{∞} represent the mass of the sample in its initial state, at time t , and in its final state, respectively.

The exact $f(\alpha)$ of solid-state reactions are often complex and/or unknown as these reactions tend to involved multiple steps with different reaction rates. Model-free iso-conversional integral methods, which can compute kinetic parameters without prior modelling assumptions, are therefore commonly used to analyse the kinetics of the solid state reactions [24]. Two kinds of iso-conversional methods, Flynn–Wall–Ozawa (FWO) and Kissinger–Akahira–Sunose (KAS) methods, were applied respectively in this study to mutually verify the results obtained by each other. Although there are a great number of the methods of kinetic analysis of non-isothermal solid state reactions other than these two methods, the FWO and KAS methods have been demonstrated with good reliability and been used widely [32].

The FWO [20] and KAS [20,33] methods are represented by:

$$\ln(\beta) = \ln[0.0048AE / R / g(\alpha)] - 1.0516E / (RT), \quad (11)$$

and

$$\ln(\beta / T^2) = \ln[AR / E / g(\alpha)] - E / RT \quad (12)$$

respectively. Therefore, by plotting $\ln(\beta)$ (FWO method) or $\ln(\beta / T^2)$ (KAS method) versus $1/T$ at selected α, the values of E can be obtained as function of the conversion degree.

3.3 Determination of the Kinetic Model Function using Master Plots Method

The lower limit of the integral in Eq. (8) that is associated with T_0 can be approximated as zero as solid-state reactions are slow at low temperature conditions. Equation (8) can therefore be simplified to [20]:

$$g(\alpha) = AE / (\beta R) \times P(u) \quad (13)$$

Whilst the integral expression $P(u) = \int_{\infty}^{u} -(e^{-u} / u^2) du$ ($u = E / RT$) in Eq. (13) cannot be solved analytically, a reasonably accurate approximation can be obtained with Doyle's rational approximation [34]:

$$P(u) = 0.00484 \exp(-1.0516u), \quad (14)$$

Using a reference at point $\alpha = 0.5$, the following equation can be derived from Eq. (13):

$$g(\alpha) / g(0.5) = P(u) / P(u_{0.5}), \quad (15)$$

where $g(0.5)$ is a constant for a given kinetic model function. Equation (15) indicates that for a given α, the value of experimentally determined reduced-generalized reaction rate $P(u)/P(u_{0.5})$ and the theoretically calculated value

of $g(\alpha)/g(0.5)$ are equivalent, when an appropriate kinetic model $f(\alpha)$ is selected to describe the rate process under investigation [29]. A comparison of the experimental plots of $P(u)/P(u_{0.5})$ against α with the theoretical plots of $g(\alpha)/g(0.5)$ against α can therefore be performed to determine the $f(\alpha)$ that provide the best agreement between the values, during the whole course of the process. A summary of the kinetic models that were applied drawn is provided in Table 2.

4 Results and discussion

4.1 Characteristics of Microalgae and Coal

As shown in Table 1, the carbon content of the microalgae sample was measured to be 47.84 wt%, which is less than the carbon content of the coal sample (66.47 wt%). This resulted in the lower heating value for the microalgae (21.88 MJ/kg) than coal (25.52 MJ/kg), as the amount of energy contained in carbon-carbon bonds is higher than that in the carbon–oxygen and carbon–hydrogen bonds, the higher measured oxygen content of the biomass, however, implies a greater thermal reactivity than the coal [35]. The microalgae was measured to have higher volatile matter (55.37 wt%) and ash (10.28 wt%) contents than the coal sample (35.12 wt% and 5.85 wt%). The volatile matter to fixed carbon ratios (VM/FCs) of the microalgae and coal samples are therefore approximated to be ~1.61 and ~0.59, respectively. Thus, the gas-phase oxidation of the volatile species is expected to be the more dominant form of combustion for the microalgae sample, which has a higher VM/FC than the coal sample [14]. In addition to that, given that the microalgae sample is found to contain a higher oxygen content and more volatile materials, which are the key elements that would

promote the initiation of ignition [36], it is anticipated that the microalgae would ignite at a lower temperature than coal.

4.2 Effect of blending ratios

The combustion characteristics of CCB*s* (MCR= 3/7, 5/5 and 7/3) and compared with pure materials are studied at β =20 °C / min. TG and DTG curves are shown in Fig.2 (a) and Fig.2 (b), respectively.

As shown in Fig.2 (a), the TG plot, the profiles of CCB are alike, yet differ from that of pure *C. vulgaris* and coal. The combustion process of CCB can be divided into three stages: the first stage is from the ambient temperature (100°C) to 254.6~ 389.4°C (depending on MCRs) , where the loss of both water and volatile compounds occurs; the second stage is from the end of the first stage to 698.7~ 741.0°C (depending on MCRs), where most volatile and carbonaceous species are burning—the main combustion process; the third stage is from the end of the second stage to 900°C, where carbonaceous residue is burning very slowly.

At the main combustion stage, the volatile matters contribute to a sufficient amount of mass loss in CCBs, leading to two regions of combustion, i.e. volatile combustion and char combustion. So there are two peaks in each DTG curve of CCB (Fig.2 (b)). In the case of CCBs, it is observed that the shape of the DTG curves was very different from the pure *C. vulgaris* and coal. The DTG curve of pure *C. vulgaris* and pure coal respectively has two big peaks and one big peak. The main combustion process of pure *C. vulgaris* is initialized at 248.3°C, and terminated at 660.8°C, which is closed to that of CCBs. Coal's burning initializes at highest temperature (408.3 °C),

and ends at highest temperature (765.1°C) compared with CCBs and pure *C. vulgaris*. The main combustion process of coal is carried out very quickly, so its DTG zone was very narrow.

Based on the TG and DTG curve analysis in Fig.2, the combustion characteristic parameters of *C. vulgaris*, coal and their blends are shown in Table 3. From Table 3 it can be seen that the ignition temperature (T_i) corresponds to the point at which the burning profile underwent a sudden rise. Final temperature (T_f) is detected as mass stabilization. Both of T_i and T_f are decreased as the *C. vulgaris* content increased in the blends. The reason is *V* content of *C. vulgaris* is higher, which is 20.25% larger than that of coal. However, its *FC* content is lower than coal. The combustion of *V* content is very easy, while the combustion of fixed carbon is difficult. And with the increasing the volatile content of *C. vulgaris* in the blends, the total content of volatile matter is also increased, while total fixed carbon content is decreased. So fuels containing large amount of volatile matter are easy to ignite, and such fuels tend to burn quickly. So it is expected that the blending of high volatile *C. vulgaris* with coal always lowers the ignition temperature and final temperature. Therefore, the combustion behavior of the blends was greatly influenced by the proportion of *C. vulgaris* in the blends.

Because the content of fixed carbon in coal is very high, so T_f of coal is highest between all samples. While compared to pure coal combustion, T_i of CCBs is lowered by 18.9-153.7 °C and T_f is lowered by 24.1-66.4 °C. This result is agreement with literature [9]. Thus, blending of *C. vulgaris* can improve the combustion

characteristics of low volatile coal, which indicates that co-combustion of *C. vulgaris* and coal is feasible.

From Table 3 it also can be seen that the maximum weight loss rate (R_{max}) of the *C. vulgaris* and blends with MCR=7/3 occur at the first peak, while R_{max} of blends with MCR=3/7 and 5/5 occurs at the second peak. R_{max} of blends with MCR=5/5 is more than that of MCR=7/3 and 3/7, but less than *C. vulgaris* and coal. Because R_{max} of *C. vulgaris* occurred at the low temperature range corresponding to the volatile combustion, while R_{max} of coal occurred at the high temperature range corresponding to the fixed carbon combustion, thus with increasing content of *C. vulgaris* in CCBs, the content of volatile is increased while the the content of fixed carbon is decreased in CCBs. And the temperature which R_{max} occurred moved from high temperature (second peak) to low temperature (first peak), and at MCR=5/5, R_{max} reached its maximum. Between all the samples, the R_{max} value of *C. vulgaris* is maximum one, indicating that the combustion of *C. vulgaris* is very fast because of its high volatile content.

The average reaction rate (R_v) of the samples is firstly decreased, and then increased as the content of *C. vulgaris* in CCBs increasing. Because the main combustion process of coal is carried out at a very narrow range, so its R_v is the highest one. R_v of CCBs is slightly decreased by 0.27-0.7%/min compared to pure coal combustion. While R_v of *C. vulgaris* is 3.87%/min, slight less than that of MCR=3/7, but more than that of MCR=5/5 and 7/3. This is because the effect of the temperature range for calculating R_v, the content of volatile and fixed carbon in CCBs

which caused the minimum R_v occurred at MCR=5/5.

Further, it can be seen from Table 3 that the residues mass (M_r) at 900 °C is first increased, and then decreased as increasing the content of *C. vulgaris* in CCBs. The maximum M_r of CCBs is obtained at MCR=5/5, while the minimum M_r is obtained at MCR=3/7. M_r of CCBs is less than pure *C. vulgaris*, but more than pure coal. This may be caused by the interaction of *C. vulgaris* and coal during co-combustion. Further research is needed to determine it, and the detailed discussion is shown at section 4.3.

Using the formula (1), (2) and (3), D_i, S and S_M can be calculated. The results are shown in Table 4. From Table 4, it can be seen that with the increasing content of *C. vulgaris*, D_i is increased,while S is first increased and then decreased. Because S is not suitable for application of biomass/coal blends mentioned in section 3.1, so S_M is better to evaluate the combustion behavior of the blends. From Table 4 it can be seen that S_M is increased as the content of *C. vulgaris* increasing in the blends. Both of D_i and S_M are increased, indicating the ignition performance and the comprehensive combustion characteristics are better as the content of *C. vulgaris* in the blends increasing. This result is agreement with that of lignite/cardoon and lignite/pine needles blends [37].

4.3 Interaction between the blends of *C. vulgaris* and coal

To further assess the interactions between the microalgae and the coal components within the blends, the theoretical DTG curves of the blends ($R_{calculated}$) at different MCR values, are calculated from the sum of decomposition curves of each individual component:

$$R_{\text{calculated}} = x_{\text{m}} R_{\text{m}} + x_{\text{c}} R_{\text{c}} \,. \tag{16}$$

In Equation 16, R_{m} and R_{c} are the mass loss rates of microalgae and coal, whereas the x_{m} and x_{c} represent the proportions of microalgae and coal within the blend, respectively. The theoretically derived curves are subsequently plotted and compared with the experimentally obtained DTG curves of the blends ($R_{\text{experimental}}$), as is shown in Fig. 3. A close agreement between the curves is expected, if there is no significant interaction between the components in the blend.

From Fig. 3, the features of the initial and the end stages of the blends are found to be similar, which indicates that the interaction of the microalgae with coal is not significant in these temperature range. Some discrepancies between the calculated and the experimental curves, however, can be observed for the blends in the middle stage of mass loss. The deviation is especially significant for the blend with a MCR of 7/3, this result is similar to both biomasses (sorghum bagasse and sugarcane bagasse) with coal blends [38] combustion. The discrepancies in the curves imply that some interactions have occurred between the two individuals, to affect the combustion processes of the blends. The interactions are especially pronounced in the higher temperature range, when a higher proportion of microalgae is present within the blend, which is the same with CBP (Composite biomass pellets) and coal at high temperature [39]. This result indicates that the increased presence of microalgae within the blend, can result in a more heterogeneous reaction rate in the higher temperature range, but with decreased intensity. This finding therefore indicates that experimental measurements must be performed to ascertain if the combustion stability and the heat

release profile of the microalgae and coal blend is within the allowable range of the combustion system, prior to use.

4.4 Effect of heating rate on the co-combustion of *C. vulgaris* and coal

The TG and DTG curves for the biomass and coal blend sample, with a MCR of 5/5, at three selected heating rates (βs) of 10, 20 and 40 °C/min are presented in Figs. 4 (a) and 4 (b), respectively. The combustion characteristic parameters of the blend at the selected βs that are derived from the plots, are also summarized in Table 5. It is noted that the biomass and coal blends are all found to display qualitatively similar characteristics for each of the heating rates considered in this study. Therefore, only the results obtained for the blend with a MCR of 5/5 are presented and discussed herein. From Fig. 4(a), it can be seen the TG curves are found to shift to higher temperature range with higher β, without any significant change their shapes. The corresponding DTG curves of the blend in Fig. 4(b) are also found to complete over a wider temperature range, in addition to shifting towards higher temperature region. The intensity of the peaks in the DTG profiles becomes more pronounced with increasing β. The shift in the temperature range implies that there may be a more significant thermal lag at higher β. This could be the result of a reduction in the time available for the whole sample to reach the same temperature as the surrounding, when a higher β is applied. It is noted that similar observations have been also reported in previous thermogravimetric investigations of various materials [40]. An increase in reactivity was noted as the heating rate increases, which indicates that combustion intensity is enhanced by higher heating rates. The increase in the intensity

of the peaks, on the other hand, implies that an enhancement in the combustion intensity of the blend when heat is supplied at a greater rate, which is to be expected.

The shift in the temperature range and the increase in the intensity of the peak are also reflected in the thermal characteristic data of the blend, which is presented in Table 5. For example, from Table 5, it can be seen that the T_i and T_f of the blend are found to shift from 244.3 to 268.8 °C, and from 685.4 to 797.5 °C, respectively, when the β was increased from 10 to 40 °C/min. The values of the first and second peaks are also measured to increase from 1.68 to 7.93 %/min, and from 3.91 to 8.56 %/min, respectively, over the same β range. It is interesting to note, however, the M_r value of the blend is found to be the least at the lowest β. The reason is that the reaction during combustion depend on the duration and intensity of heating of the substrate. Thus, different heating rates produce different end products. At higher heating rates, because lack of sufficient time for the consecutive reactions occurrence and reduction in heat transfer efficiency from the surface to the core of the sample, it will result less complete decomposition and more M_r produced of the sample when higher heating rate was applied [40]. Besides, the variation of M_r at higher heating rates (20 and 40°C/min) is minimal. This result is similar to two kinds of autotrophic microalgae (*Spirulina platensis* and *Chlorella protothecoides*) [19].

4.5 Kinetics analysis

To further evaluate the effect of the blending ratio on the characteristics of the fuel samples from T_i to T_f, the FWO (Eq. 11) and KAS (Eq. 12) methods were used to compute the kinetics parameters (E). Table 6 shows the value of the kinetic parameter

(E) that are derived using both FWO and KAS methods, and their corresponding linear correlation factors (R^2). From the table, it can be seen that the values of R^2 are within the range of 0.91939 and 1.00.

From Table 6, the values of E for all fuels are observed decrease gradually as the conversion degree increases. Besides, with the increasing content of *C.vulgaris* in the blends, the E of blends is the first reduced, and then increased. The E values of blends of Indian coal mixing with treated municipal solid waste also has the same trend [41]. This is because the temperature range for calculated E of *C.vulgaris* is wider than that of coal, so the E values of blends is increased (except MCR=3/7) with increasing the content of *C.vulgaris*. However, at MCR=3/7, the E value reaches its maximum. This result indicates that the 30% *C.vulgaris* is not suitable for co-firing with coal.

The E value of coal ranging from 44.81 to 78.29 kJ/mol, which is of similar magnitude to the E value reported for a semi-anthracite coal sample (84.59 kJ/mol), which has a similar carbon content (63.15 wt%) [36]. The burning of the microalgae and the blends, on the other hand, display greater E range between 55.72 and 163.54 kJ/mol.

For the blends, the average value of E derived by FWO and KAS methods is ranged from 85.28 kJ/mol to 108.99 kJ/mol, and the minimum E is obtained as MCR= 5/5. This means that blend with MCR= 5/5 is favorable to ensure lower activation energy resulting in lower temperature requirement for promotion of combustion.

For the pure *C.vulgaris*, its average E is 104.98 kJ/mol, which is more 42.08 kJ/mol than that of pure coal. This indicates that the coal sample has a better reactivity

than microalgae in the temperature ranged from T_i to T_f, which is consistent with the earlier results presented in Section 4.2. It is noteworthy that there are many studies that have observed lower E for their coal samples, when compared with the biomass samples that they were investigating, which include forest residual, cotton residual, wood [9], microalgae [25], and vice versa. The discrepancies in the trends reported in the literature can be attributed to different factors, such as the properties of the investigated fuels and the operating parameters used [25]. Care must therefore be taken before making direct comparisons.

As is noted in Section 3.3, the experimentally determined value of the reduced-generalized reaction rate $P(u)/P(u_{0.5})$ and the theoretically calculated value of $g(\alpha)/g(0.5)$ are equivalent when an appropriate $f(\alpha)$ is applied to describe the rate process under investigation. Using the average value of E calculated by KAS and FWO method, along with the temperature measured during the experiments, the $P(u)$ can subsequently be derived using Eq. (14). The experimental master plots of $P(u)/P(u_{0.5})$ versus α for *C.vulgaris*, coal and their blends, at three selected β values of 10, 20, and 40°C/min, are presented in Fig. 5. From Fig. 5, it can be seen that the experimental master-plots for the same fuel, at different heating rates, are similar in features. This implies that their combustion kinetics at different heating rates could be represented using a single kinetic model [20]. Comparisons are therefore only made between the theoretically derived $g(\alpha)/g(0.5)$ for several kinetic functions (Table 2), and the experimentally derived $P(u)/P(u_{0.5})$, for the data recorded at a β value of 20 °C/min, in Fig. 6.

From Fig. 6, it can be seen that an exact match between the theoretical master plots and the experimental master-plots is not obtained. Nonetheless, the comparison reveals that the characteristics of the experimental master-plots of microalgae and the blends may have some similarities with the behaviours of the theoretical master-plots generated using the F_n kinetic functions, which are close the theoretical master-plots of F_2 or F_3.

The experimental master-plot of the coal sample is also observed to display some resemblances with the theoretical master-plots generated using kinetic functions of F_1 and F_2, or D_1 and D_2 from Table 2. To further determine the F_n or the D_n models that better match the experimental data of coal, plots of $g(\alpha)/g(0.5)$ versus α, using F_n and D_n models, for n =1 and 2, are therefore plotted against the experimental master-plots of the coal sample in Figs. 7(a) and Figs. 7(b), respectively. Similarly, plots of $g(\alpha)/g(0.5)$ versus α generated using F_n models, for n values ranging from 2 to 10, are also plotted against the experimental master-plots of the microalgae and the blends in Fig. 7(c). From the figures, it can be seen that the experimental master-plot of coal displays a closer agreement with the theoretical master-plots that were generated using kinetic functions of F_1 and F_2.

The experimental master-plots of the microalgae and the blends, on the other hand, are observed to reside between the theoretical master-plots that were generated using kinetic functions of F_2 and F_5. Together, these findings indicate that the kinetic processes of coal, microalgae and their blends are best represented using $g(\alpha) = [(1-\alpha)^{1-n} - 1]/(n-1)$. Equation (13) can therefore be expressed as:

$$g(\alpha) = AE/(\beta R) \times P(u) = [(1-\alpha)^{1-n} - 1]/(n-1) \quad (17)$$

By plotting $[(1-\alpha)^{1-n} - 1]/(n-1)$ versus $E/(\beta R) \times P(u)$ for different values of n, the method of least square can therefore be used to determine the most optimal value of n (highest R^2 and lowest intercept value) for each fuel. The pre-exponential factors (A) can also be derived from the slopes of the plots. The kinetic triplets (E, n and A) of the pure coal, blends with MCR of 3/7, 5/5, 7/3 and pure microalgae *C. vulgaris* combustion at β=20 °C/min are respectively E=62.90, 108.99, 85.28, 92.27, 104.98 kJ/mol, n =1.4, 4.1, 2.7, 3.2, 4 and A =6.38×10^5, 1.05×10^6, 2.29×10^4, 8.73×10^4, 2.93×10^6 min^{-1}. R^2 is within the range of 0.99909 and 0.99950.

5 Conclusions

Three stages of CCBs during the combustion can be distinguished, and the main combustion stages are ranged from 254.6~ 389.4°C to 698.7~ 741.0°C (depending on MCRs) . R_{max} of *C. vulgaris* is maximum one. R_v of blend with MCR=5/5 is minimum one. Both of D_i and S_M are increased as increasing the content of *C. vulgaris* in CCBs. Slight interaction was observed during the co-combustion of *C. vulgaris* and coal. As β increases, T_i, T_p, R_p ,R_v and T_f are all increased significantly. MCR= 3/7 is not suitable for co-firing, while MCR= 5/5 is favorable to ensure lower activation energy. The kinetic triplets are obtained by the Kissinger–Akahira–Sunose (KAS), Flynn–Wall–Ozawa (FWO), and master-plots method, they are respectively E=62.90, 108.99, 85.28, 92.27, 104.98kJ/mol, n =1.4, 4.1, 2.7, 3.2, 4 and A =6.38×10^5, 1.05×10^6, 2.29×10^4, 8.73×10^4, 2.93×10^6 min^{-1} for the coal, blends with MCR of 3/7, 5/5, 7/3 and *C. vulgaris* combustion at β=20 °C/min. The The combustion characteristics and

kinetic results presented are important to help explain and predict the behavior of the microalgae and its blends with coal, in practical applications.

Acknowledgments

This work is supported by Guangxi Natural Science Foundation (2014GXNSFBA118252), Guangxi Scientific Research and Technology Development Project (Gui Kegong 1598008-17), University scientific research key project of Guangxi Zhuang Autonomous Region Education Department (ZD2014008) and the Australian Research Council (ARC Discovery DP150104395 and ARC Linkage LP140100817).

References

[1] H. Zhou, et al., Experimental investigation of ignition and combustion characteristics of single coal and biomass particles in O_2/N_2 and O_2/H_2O, J. Energy Inst. (2018), https://doi.org/10.1016/j.joei.2018.04.008.

[2] Tagliaferro G. V., Filho H.J.I., Chandel A.K., et al., Continuous cultivation of Chlorella minutissima 26a, in a tube-cylinder internal-loop airlift photobioreactor to support 3G biorefineries, Renew. Energy 130(2018)439-445.https://doi.org/10.1016/j.renene.2018.06.041.

[3] Chen, C., et al., Emissions characteristics of NO_x and SO_2 in the combustion of microalgae biomass using a tube furnace, J. Energy Inst. 90 (2017)806-812. http://dx.doi.org/10.1016/j.joei.2016.06.003.

[4] Wu, Z., et al., Synergistic effects from co-pyrolysis of low-rank coal and model components of microalgae biomass, Energ. Convers. Manage. 135(2017) 212-225. https://doi.org/10.1016/j.enconman.2016.12.060.

[5] Grierson S., Strezov V., Ellem G., Mcgregor R., Herbertson J., Thermal characterisation of microalgae under slow pyrolysis conditions, J. Anal. Appl. Pyrolysis. 85 (2009) 118-123.

https://doi.org/10.1016/j.jaap.2008.10.003.

[6] Chen C., Ma X., He Y., Co-pyrolysis characteristics of microalgae Chlorella vulgaris and coal through TGA, Bioresour. Technol. 117 (2012) 264-273. https://doi.org/10.1016/j.biortech.2012.04.077.

[7] Mata, T.M., Martins, A.A., Caetano, N.S., Microalgae for biodiesel production and other applications: A review, Renew. Sust. Energ. Rev. 14 (2010)217-232. https://doi.org/10.1016/j.rser.2009.07.020.

[8] Medwell, P.R., Nathan, G.J., Chan, Q.N., Alwahabi, Z.T., Dally, B.B., The influence on the soot distribution within a laminar flame of radiation at fluxes of relevance to concentrated solar radiation, Combust. Flame 158(2011) 1814-1821. https://doi.org/10.1016/j.combustflame.2011.01.006.

[9] Kastanaki E., Vamvuka D., A comparative reactivity and kinetic study on the combustion of coal–biomass char blends, Fuel 85(2006)1186–1193. https://doi.org/10.1016/j.fuel.2005.11.004.

[10] X. Wang, et al., Influence of coal co-firing on the particulate matter formation during pulverized biomass combustion, J. Energy Inst. (2018), https://doi.org/10.1016/j.joei.2018.05.003.

[11] Hu S., Ma X., Lin Y., Yu Z., Fang S., Thermogravimetric analysis of the co-combustion of paper mill sludge and municipal solid waste, Energ. Convers. Manage. 99(2015)112-118. https://doi.org/10.1016/j.enconman.2015.04.026.

[12] Biagini E., Lippi F., Petarca L., Tognotti L., Devolatilization rate of biomasses and coal–biomass blends: an experimental investigation, Fuel 81(2002) 1041–1050. https://doi.org/10.1016/S0016-2361(01)00204-6.

[13] Saidur R., Abdelaziz E.A., Demirbas A., Hossain M.S., Mekhilef S., A review on biomass as a fuel for boilers, Renew Sust. Energ. Rev.15(2011) 2262-2289. https://doi.org/10.1016/j.rser.2011.02.015.

[14] Wang C., Wang F., Yang Q., Liang R., Thermogravimetric studies of the behavior of wheat straw with added coal during combustion, Biomass Bioenergy 33(2009) 50-56. https://doi.org/10.1016/j.biombioe.2008.04.013.

[15] Theis M., Skrifvars B.J., Hupa M., Tran H., Fouling tendency of ash resulting from burning

mixtures of biofuels. Part 1: Deposition rates, Fuel 85(2006)1125–1130. https://doi.org/10.1016/j.fuel.2005.10.010.

[16] Xie Q.S., Study on the combustion and pollutant emission characteristics of coal blent with biomass in O_2/CO_2 atmosphere, School of energy and power engineering. 2012, Shandong Unversity: Shan dong. 1-85.(In Chinese)

[17] Ong S.C., Kao C.Y., Chiu S.Y., Tsai M.T., Lin C.S., Characterization of the thermal-tolerant mutants of Chlorella sp with high growth rate and application in outdoor photobioreactor cultivation, Bioresour. Technol. 101(2010)2880-2883. https://doi.org/10.1016/j.biortech.2009.10.007.

[18] Chinnasamy S., Bhatnagar A., Hunt R.W., Das K.C., Microalgae cultivation in a wastewater dominated by carpet mill effluents for biofuel applications, Bioresour. Technol. 101(2010)3097-3105. https://doi.org/10.1016/j.biortech.2009.12.026.

[19] Peng W.M., Wu Q.Y., Tu P.G., Zhao N., Pyrolytic characteristics of microalgae as renewable energy source determined by thermogravimetric analysis, Bioresour. Technol. 80(2001) 1-7. https://doi.org/10.1016/S0960-8524(01)00072-4.

[20] Zou S.P., Wu Y.L., Yang M.D., Li C., Tong J.M., Pyrolysis characteristics and kinetics of the marine microalgae Dunaliella tertiolecta using thermogravimetric analyzer, Bioresour. Technol. 101(2010)359-365. https://doi.org/10.1016/j.biortech.2009.08.020.

[21] Sanchez-Silva L., López-González D., Garcia-Minguillan A.M., Valverde J.L., Pyrolysis, combustion and gasification characteristics of Nannochloropsis gaditana microalgae, Bioresour. Technol. 130(2013)321-331. https://doi.org/10.1016/j.biortech.2012.12.002.

[22] Agrawal A., Chakraborty S., A kinetic study of pyrolysis and combustion of microalgae Chlorella vulgaris using thermo-gravimetric analysis, Bioresour. Technol. 128(2013)72-80. https://doi.org/10.1016/j.biortech.2012.10.043.

[23] Tang Y.T., Ma X.Q., Lai Z.Y., Thermogravimetric analysis of the combustion of microalgae and microalgae blended with waste in N_2/O_2 and CO_2/O_2 atmospheres, Bioresour. Technol. 102(2011)1879–1885. https://doi.org/10.1016/j.biortech.2010.07.088.

[24] Chen, C.X., Ma X.Q., Liu K., Thermogravimetric analysis of microalgae combustion under different oxygen supply concentrations, Appl. Energ. 88(2011) 3189-3196. https://doi.org/10.1016/j.apenergy.2011.03.003.

[25] Tahmasebi A., Kassim M.A., Yu J.L., Bhattacharya S., Thermogravimetric study of the combustion of Tetraselmis suecica microalgae and its blend with a Victorian brown coal in O_2/N_2 and O_2/CO_2 atmospheres, Bioresour. Technol. 150(2013)15-27. https://doi.org/10.1016/j.biortech.2013.09.113.

[26] Y. Gao, et al., Combustion characteristics and air pollutant formation during oxy-fuel co-combustion of microalgae and lignite, Bioresour. Technol. 207(2016)276-284. https://doi.org/10.1016/j.biortech.2016.02.031.

[27] Sahu S.G., Sarkar P., Chakraborty N., Adak A.K., Thermogravimetric assessment of combustion characteristics of blends of a coal with different biomass chars, Fuel Process Technol. 91(2010)369–378. https://doi.org/10.1016/j.fuproc.2009.12.001.

[28] Pu G., Zhu W.L., Zhou H.P., Lei Q., Zhang Z.R., Liu J.J., Co-Combustion Characteristics of Inferior Coal and Biomass Blends in an Oxygen-Enriched Atmosphere, BioResour. 10(2015)1452-1461. https://DOI: 10.15376/biores.10.1.1452-1461

[29] Cai J.M., Liu R.H., Kinetic analysis of solid-state reactions: Precision of the activation energy obtained from one type of integral methods without neglecting the low temperature end of the temperature integral, Solid State Sci. 10(2008) 659-663. https://doi.org/10.1016/j.solidstatesciences.2007.10.018.

[30] Zuru A.A., Dangoggo S.M., Birnin-Yauri U.A., Tambuwal A.D., Adoption of thermogravimetric kinetic models for kinetic analysis of biogas production, Renew Energy 29(2004)97-107. https://doi.org/10.1016/S0960-1481(03)00074-0.

[31] Xiao H.M., Ma X.Q., Lai Z.Y., Isoconversional kinetic analysis of co-combustion of sewage sludge with straw and coal, Appl. Energ. 86(2009) 1741-1745. https://doi.org/10.1016/j.apenergy.2008.11.016.

[32] Tanaka H., Thermal analysis and kinetics of solid state reactions, Thermochim Acta. 267(1995) 29-44. https://doi.org/10.1016/0040-6031(95)02464-6.

[33] Boonchom B., Puttawong S., Thermodynamics and kinetics of the dehydration reaction of $FePO_4 . 2H_2O$, Physica B 405(2010) 2350-2355. https://doi.org/10.1016/j.physb.2010.02.046.

[34] Doyle C.D., Estimating isothermal life from thermogravimetric data, J. Appl. Polym. Sci. 6(1962)639–642. https://doi.org/10.1002/app.1962.070062406.

[35] Wang G., Zhang J., Shao J., Liu Z., Zhang G., Xu T., et. al., Thermal behavior and kinetic

analysis of co-combustion of waste biomass/low rank coal blends, Energ. Convers. Manage. 124(2016)414-426. https://doi.org/10.1016/j.enconman.2016.07.045.

[36] Liao Y.F., Ma X.Q., Thermogravimetric analysis of the co-combustion of coal and paper mill sludge, Appl. Energ. 87(2010) 3526-3532. https://doi.org/10.1016/j.apenergy.2010.05.008.

[37] Vamvuka D., Sfakiotakis S., Combustion behaviour of biomass fuels and their blends with lignite, Thermochim Acta. 526(2011) 192-199. https://doi.org/10.1016/j.tca.2011.09.021.

[38] N.R. Galina, et al., Comparative study on combustion and oxy-fuel combustion environments using mixtures of coal with sugarcane bagasse and biomass sorghum bagasse by the thermogravimetric analysis, J. Energy Inst. (2018), https://doi.org/10.1016/j.joei.2018.02.008

[39] F.H. Guo, Z.P Zhong, Optimization of the co-combustion of coal and composite biomass Pellets, J. Clean. Prod. 185 (2018)399-407. https://doi.org/10.1016/j.jclepro.2018.03.064.

[40] Bada S.O., Falcon R.M.S., Falcon L.M., Makhula M.J., Thermogravimetric investigation of macadamia nut shell, coal, and anthracite in different combustion atmospheres, J. S. Afr. Inst. Min. Metall. 115 (2015) 741-746. https://DOI: 10.17159/2411-9717/2015/V115N8A10.

[41] Muthuraman M., Namioka T., Yoshikawa K., A comparative study on co-combustion performance of municipal solid waste and Indonesian coal with high ash Indian coal: A thermogravimetric analysis, Fuel Process. Technol. 91 (2010) 550–558. https://doi.org/10.1016/j.fuproc.2009.12.018.

Figure captions

Fig.1. Schematic diagram of the experimental setup used for thermogravimetric analysis.

Fig.2(a) TG curves of microalgae, coal and their blends with microalgae to coal ratio (MCR) of 3/7, 5/5 and 7/3, under a heating rate (β) of 20 °C/min.

Fig.2(b) DTG curves of microalgae, coal and their blends with microalgae to coal ratio (MCR) of 3/7, 5/5 and 7/3, under a heating rate (β) of 20 °C/min.

Fig.3(a) Comparisons of the calculated with the experimental observed DTG profiles of the blends with MCR of 3/7, under a β of 20 °C/min.

Fig.3(b) Comparisons of the calculated with the experimental observed DTG profiles of the blends with MCR of 5/5, under a β of 20 °C/min..

Fig.3(c) Comparisons of the calculated with the experimental observed DTG profiles of the blends with MCR of 7/3, under a β of 20 °C/min.

Fig.4(a). TG curves of the blend with MCR of 5/5 at three selected βs of 10, 20 and 40°C/min.

Fig.4(b). DTG curves of the blend with MCR of 5/5 at three selected βs of 10, 20 and 40°C/min.

Fig.5(a) The experimental master-plots $P(u)/P(u_{0.5})$ versus the degree of conversion (α) for the coal, at three selected βs of 10, 20 and 40°C/min.

Fig.5(b) The experimental master-plots $P(u)/P(u_{0.5})$ versus the degree of conversion (α) for the blends with MCR of 3/7, at three selected βs of 10, 20 and 40°C/min.

Fig.5(c) The experimental master-plots $P(u)/P(u_{0.5})$ versus the degree of conversion (α) for the blends with MCR of 5/5, at three selected βs of 10, 20 and 40°C/min..

Fig.5(d) The experimental master-plots $P(u)/P(u_{0.5})$ versus the degree of conversion (α) for the blends with MCR of 7/3, at three selected βs of 10, 20 and 40°C/min.

Fig.5(e) The experimental master-plots $P(u)/P(u_{0.5})$ versus the degree of conversion (α) for the microalgae, at three selected βs of 10, 20 and 40°C/min.

Fig.6. The theoretical master-plots $g(\alpha)/g(0.5)$ and the experimental master plots $P(u)/P(u_{0.5})$ versus α for the different fuel samples under β of 20°C/min

Fig.7(a) The experimental master-plots $P(u)/P(u_{0.5})$ and the theoretical master-plots $g(\alpha)/g(0.5)$ of the coal sample, generated using F_n model, versus α of the sample, under a β of 20°C/min.

Fig.7(b) The experimental master-plots $P(u)/P(u_{0.5})$ and the theoretical master-plots $g(\alpha)/g(0.5)$ of the coal sample, generated using D_n model, versus α of the sample, under a β of 20°C/min.

Fig.7(c) The experimental master-plots $P(u)/P(u_{0.5})$ and the theoretical master-plots $g(\alpha)/g(0.5)$ of the microalgae and blends, generated using F_n model, versus α of the sample, under a β of 20°C/min.

Tables

Table 1

Ultimate analysis, proximate analysis and lower heating values of *C. vulgaris* and coal (dry basis).

Samples	Ultimate analysis (wt %)					Proximate analysis (wt %)			$Q_{net,d}$[a](MJ/kg)
	C	H	O[b]	N	S	V[c]	A[d]	FC[e]	
C. vulgaris	47.84	6.41	25.00	9.01	1.46	55.37	10.28	34.35	21.88
Coal	66.47	4.76	20.84	0.96	1.12	35.12	5.85	59.03	25.52

[a] $Q_{net,d}$: Lower heating value on dry basis

[b] Calculated by difference, O (%) = 100-C-H-N-S-ash

[c] V: Volatile matters

[d] A: Ash

[e] FC: Fixed carbon

Table 2

Commonly used kinetic model functions to describe solid state processes.

Mechanisms	Symbol	$F(\alpha)$	$g(\alpha)$
Order of reaction			
First-order	F_1	$1-\alpha$	$-\ln(1-\alpha)$
Second-order	F_2	$(1-\alpha)^2$	$(1-\alpha)^{-1}-1$
Third-order	F_3	$(1-\alpha)^3$	$[(1-\alpha)^{-2}-1]/2$
Diffusion			
One-way transport	D_1	0.5α	α^2
Two-way transport	D_2	$[-\ln(1-\alpha)]^{-1}$	$\alpha+(1-\alpha)\ln(1-\alpha)$
Three-way transport	D_3	$1.5(1-\alpha)^{2/3}[1-(1-\alpha)^{1/3}]^{-1}$	$[1-(1-\alpha)^{1/3}]^2$
Ginstling-Brounshtein equation	D_4	$1.5(1-\alpha)^{1/3}-]^{-1}$	$(1-2\alpha/3)-(1-\alpha)^{2/3}$
Limiting surface reaction between both phases			
One dimension	R_1	1	α
Two dimensions	R_2	$2(1-\alpha)^{1/2}$	$1-(1-\alpha)^{1/2}$
Three dimensions	R_3	$3(1-\alpha)^{2/3}$	$1-(1-\alpha)^{1/3}$
Random nucleation and nuclei growth			
Two-dimensional	A_2	$2(1-\alpha)\,[-\ln(1-\alpha)]^{1/2}$	$[-\ln(1-\alpha)]^{1/2}$
Three-dimensional	A_3	$3(1-\alpha)\,[-\ln(1-\alpha)]^{2/3}$	$[-\ln(1-\alpha)]^{1/3}$
Exponential nucleation			
Power law, $n = 1/2$	P_2	$2\alpha^{1/2}$	$\alpha^{1/2}$
Power law, $n = 1/3$	P_3	$3\alpha^{2/3}$	$\alpha^{1/3}$
Power law, $n = 1/4$	P_4	$4\alpha^{3/4}$	$\alpha^{1/4}$

Table 3

Combustion characteristic parameters of *C. vulgaris*, coal and their blends, under a heating rate (β) of 20 °C/min.

Samples	T_i[f](°C)	T_p[g](°C)		R_p[h](%/min)		R_v[i](%/min)	T_f[j](°C)	M_r[k](%)
		T_{p1}[l]	T_{p2}[m]	R_{p1}[n]	R_{p2}[o]			
Pure coal	408.3	525.7	-	6.87	-	4.22	765.1	6.83
MCR= 3/7	389.4	286.0	538.5	2.38	6.56	3.95	741.0	7.51
MCR= 5/5	255.6	285.0	530.8	3.98	6.69	3.52	711.1	12.32
MCR= 7/3	254.6	282.1	572.6	5.70	5.19	3.70	698.7	8.77
Pure *C. vulgaris*	248.3	279.3	569.1	7.92	6.13	3.87	660.8	12.56

[f] T_i: Ignition temperature

[g] T_p: Peak temperature

[h] R_p: Reaction rate at the peaks

[i] R_v: Average reaction rate during the temperature ranging from the ignition temperature to the final temperature

[j] T_f: Temperature (final) detected when stabilization of samples mass occurred

[k] M_r: Residual mass at 900°C

[l] T_{p1}: Temperature of the first major peak

[m] T_{p2}: Temperature of the second major peak

[n] R_{p1}: Reaction rate for the first major peak

[o] R_{p2}: Reaction rate for the second major peak

Table 4

Ignition index (D_i) and comprehensive combustion characteristic index (S) for the *C. vulgaris*, coal and their blends, under a heating rate (β) of 20 °C/min.

Samples	t_i[p] (min)	R_{max}[q] (%/min)	t_m[r] (min)	D_i(%/min)	$S\times10^7$ ($\%^2/(min^2/°C^3)$)	$S_M\times10^7$ ($\%^2/(min^2/°C^3)$)
Pure coal	27.23	6.87	33.1	5.65	2.27	-
MCR= 3/7	26.3	6.56	33.8	3.42	2.31	1.57
MCR= 5/5	19.89	6.69	33.4	3.98	5.07	4.04
MCR= 7/3	19.6	5.7	21.1	5.29	4.66	4.45
Pure *C. vulgaris*	19.58	7.92	21	7.38	7.52	-

[p] t_i: Ignition time, which corresponds to ignition temperature (T_i)

[q] R_{max}: Maximum combustion rate

[r] t_m: Time that corresponds to the maximum combustion rate

Table 5
Combustion characteristic parameters of the blend with a microalgae to coal ratio (MCR) of 5/5 at three selected heating rates (βs).

Sample	β (°C/min)	T_i(°C)	T_p(°C)		R_p(%/min)		R_v(%/min)	T_f(°C)	M_r(%)
			T_{p1}	T_{p2}	R_{p1}	R_{p2}			
MCR = 5/5	10	244.3	275.7	513.4	1.68	3.91	1.85	685.4	9.90
	20	255.6	285.0	530.8	3.98	6.69	3.52	711.1	12.32
	40	268.8	300	576.0	7.93	8.56	6.35	797.5	11.68

Table 6

Activation energy (E) values for different degree of conversion (α) of the samples, derived using the Flynn–Wall–Ozawa (FWO) and Kissinger–Akahira–Sunose (KAS) methods.

Samples	α	FWO method		KAS method	
		E(kJ/mol)	R^2	E(kJ/mol)	R^2
Pure coal	0.2	77.76	0.99325	71.19	0.99042
	0.3	78.29	1	66.26	0.99776
	0.4	72.96	0.99852	61.52	1
	0.5	68.5	1	57	0.99814
	0.6	64.4	0.99884	52.71	0.99289
	0.7	60.64	0.9959	48.65	0.9847
	0.8	55.92	0.98987	44.81	0.97377
	Average	**68.35**		**57.45**	
MCR=3/7	0.2	163.54	0.99325	162.72	0.97747
	0.3	141.13	0.97959	132.73	0.9635
	0.4	132.99	0.92308	111.12	0.95061
	0.5	109.42	0.94936	94.82	0.93873
	0.6	98.03	0.93557	82.07	0.92756
	0.7	84.49	0.95301	71.8	0.91681
	0.8	77.58	0.94232	63.33	0.90613
	Average	**115.31**		**102.66**	
MCR=5/5	0.2	121.28	0.9959	115.28	0.99682
	0.3	99.36	0.99726	100.83	0.98839
	0.4	97.23	0.97581	88.81	0.97721
	0.5	88.07	0.96428	78.66	0.96446
	0.6	80.35	0.95301	69.97	0.95063
	0.7	70.46	0.96428	62.41	0.93569
	0.8	65.43	0.95523	55.72	0.91939
	Average	**88.88**		**81.67**	
MCR=7/3	0.2	121.28	0.9959	119.39	0.99744
	0.3	108.16	0.98684	106.62	0.9986
	0.4	99.36	0.99726	95.87	0.99932
	0.5	91.33	1	86.67	0.99974
	0.6	91.33	1	78.64	0.99994
	0.7	78.29	1	71.51	1
	0.8	78.29	1	65.08	0.99992
	Average	**95.43**		**89.11**	
Pure *C. vulgaris*	0.2	147.54	0.94232	154.02	0.92826
	0.3	134.21	0.97959	131.33	0.96319
	0.4	117.43	0.96428	112.9	0.98196
	0.5	99.36	0.99726	97.94	0.99204
	0.6	90.5	0.99082	85.62	0.99724
	0.7	84.14	0.99804	75.28	0.99954
	0.8	72.96	0.99852	66.43	0.99996
	Average	**106.59**		**103.36**	

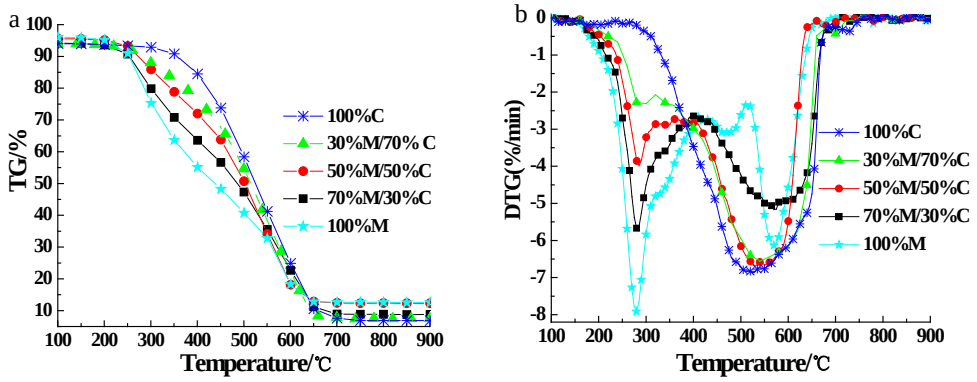

Fig.1. The (a) TG and the (b) DTG curves of microalgae, coal and their blends with microalgae to coal ratio (MCR) of 3/7, 5/5 and 7/3, under a heating rate (β) of 20 °C/min.

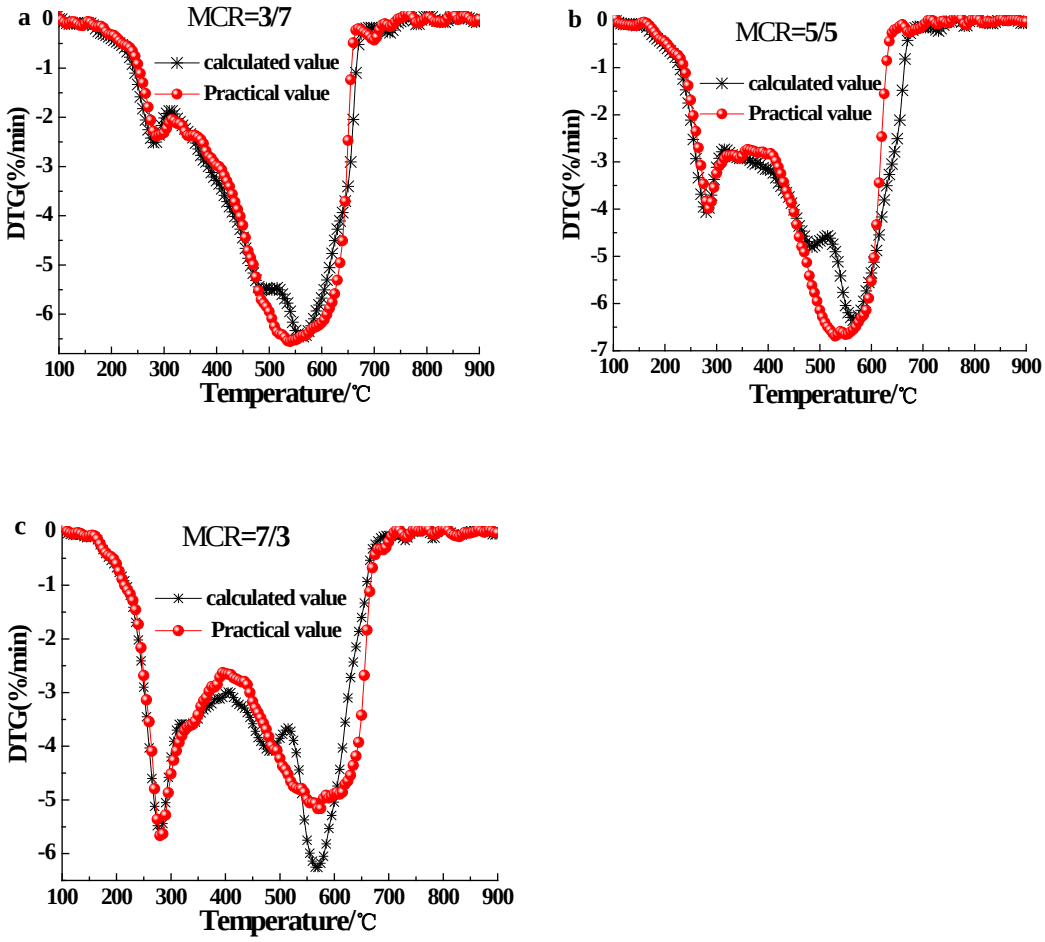

Fig.2. Comparisons of the calculated with the experimental observed DTG profiles of the blends with MCR of (a): 3/7, (b): 5/5, and (c):7/3 under a β of 20 °C/min.

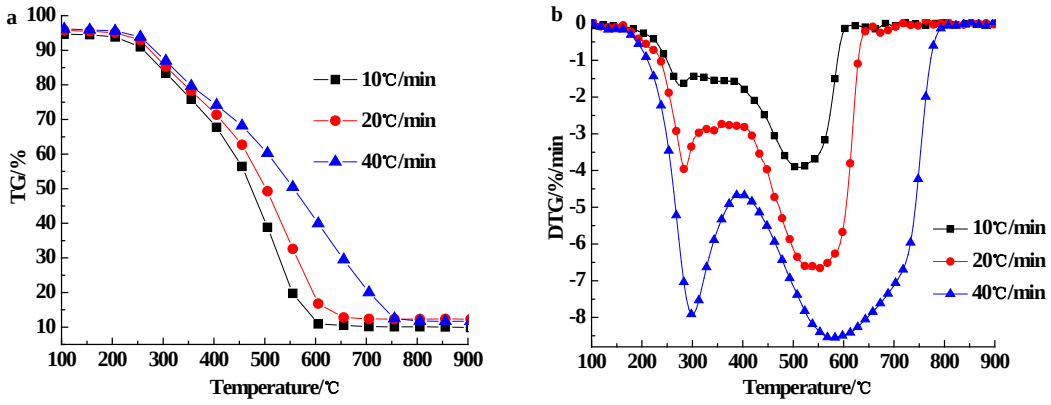

Fig.3. The (a) TG and the (b) DTG curves of the blends with MCR of 5/5, at three selected βs of 10, 20 and 40°C/min.

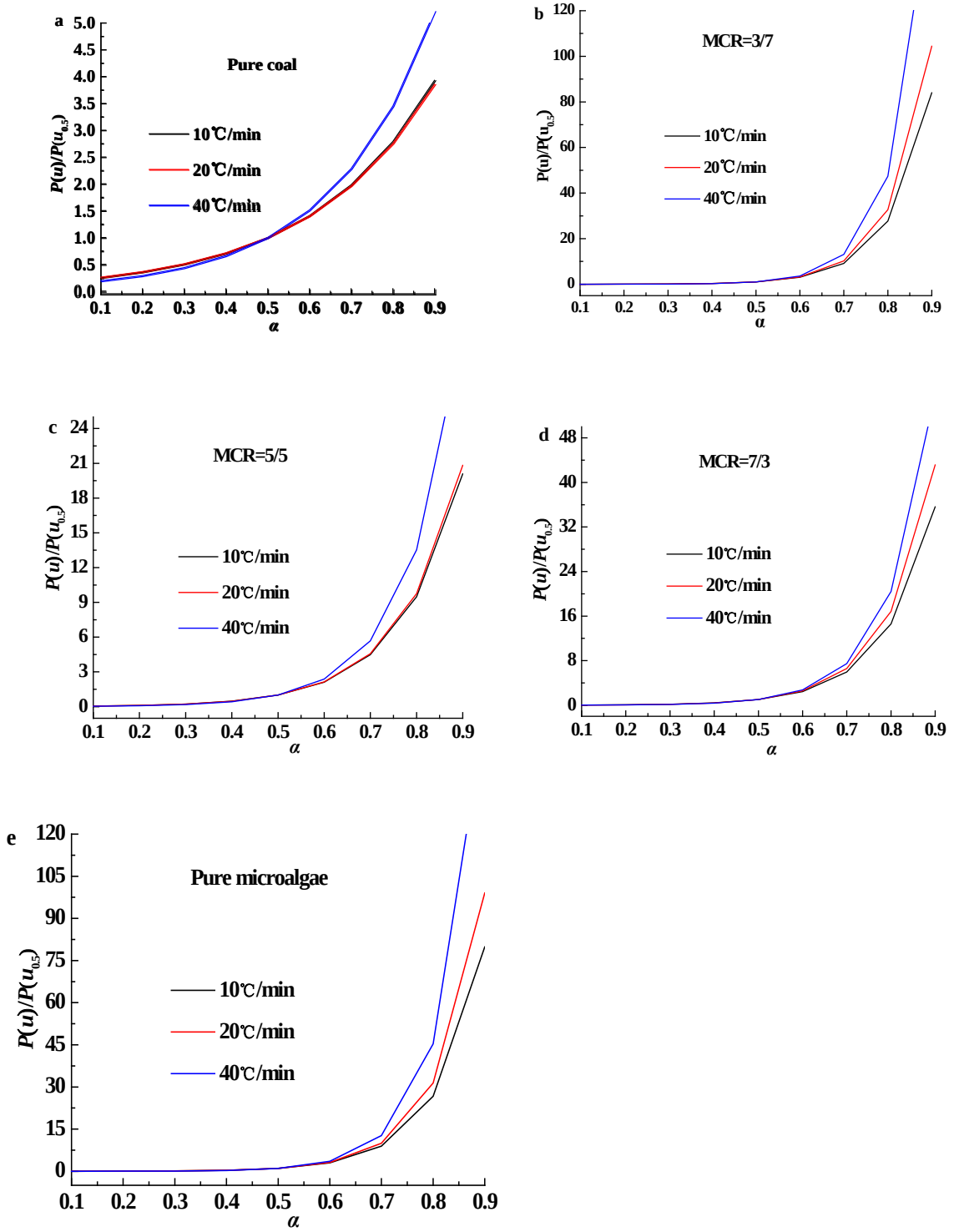

Fig.4. The experimental master-plots $P(u)/P(u_{0.5})$ versus α for the (a): coal, blends with MCR of (b)**:** 3/7, (c):5/5, (d): 7/3, and (e): microalgae, at three selected βs of 10, 20 and 40°C/min.

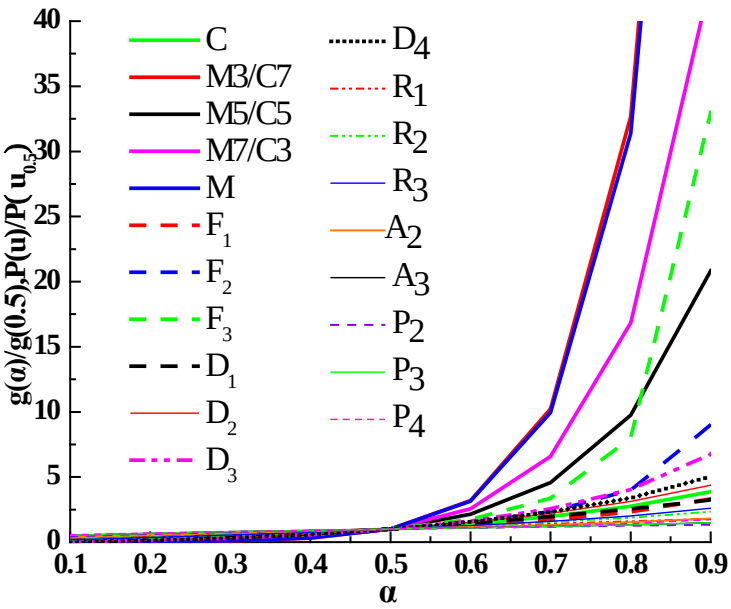

Fig.5. The theoretical master-plots $g(\alpha)/g(0.5)$ and the experimental master plots $P(u)/P(u_{0.5})$ versus α for the different fuel samples under β of 20°C/min.

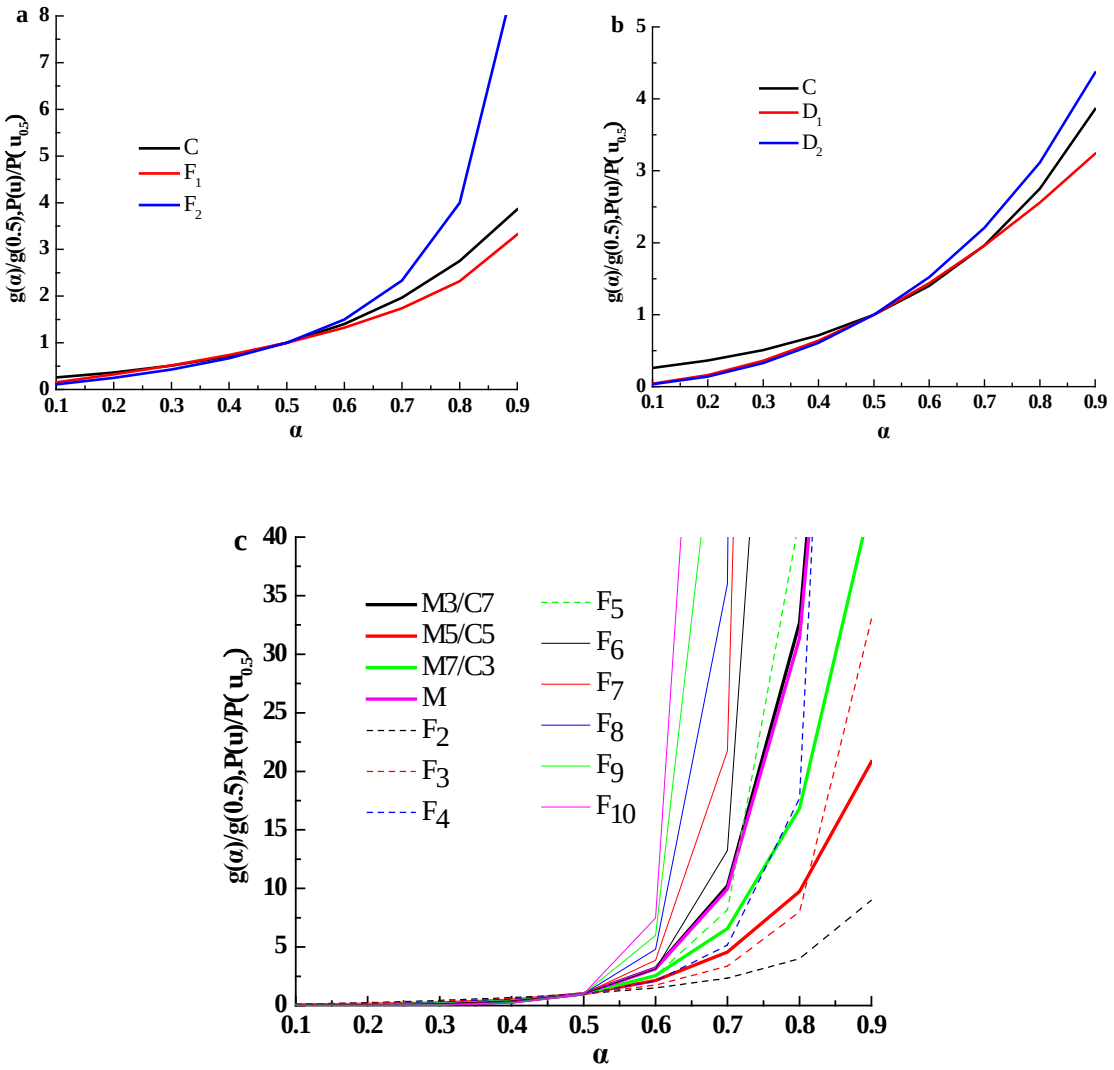

Fig.6. The experimental master-plots $P(u)/P(u_{0.5})$ and the theoretical master-plots $g(\alpha)/g(0.5)$ of the coal sample, generated using (a): F_n or (b): D_n model, versus α of the sample. (c): The $P(u)/P(u_{0.5})$ and the $g(\alpha)/g(0.5)$ plots of the microalgae and blends, generated using F_n model, versus α of the samples. The experiments were performed under a β of 20°C/min.